Euler Solutions for Highly Loaded Turbine Cascades

B. N. Srivastava*
Avco Everett Research Laboratory Inc., Everett, Massachusetts
and
R. Bozzola†
Avco Lycoming Division, Stratford, Connecticut

This paper discusses the numerical formulation aspects of computing flowfields in several highly loaded turbine cascades. The theoretical formulation for the integration of the Euler equations utilizes a generalized transformed body-fitted coordinate system and an unsplit explicit MacCormack's scheme (based on centered flux balancing) to achieve steady-state solutions. Computational results have been generated for subsonic and transonic flows in several high-turning-angle and high-solidity turbine cascades that are representative of advanced turbine technology. The results of the computational simulation have been favorably compared with measured surface pressure data, outflow angles, and outflow Mach numbers for C- and H-grid topologies.

I. Introduction

THE complexity of the flow processes in gas turbine engine components has motivated the development of computational methods as design analysis tools. In particular, an accurate and cost-effective three-dimensional viscous solution technique to predict flow behavior in cascade flowfields is a very useful design and analysis tool for gas turbine engine applications. Three-dimensional viscous cascade flow computation can be broken up into several selected technical efforts that address key aspects of the overall problem. One of these tasks relates to the modeling issues of the flow in a high-solidity and high-turning-angle cascade (as is found in highly loaded turbine stages). There are several critical numerical issues that demand careful study in the context of a highly loaded cascade geometry. These are issues that are introduced due to the specific geometrical complexity and are generally not encountered in the context of a simple problem.[1-3]

This paper deals with the details of such an effort related to a two-dimensional Euler cascade code formulation that has been developed as a step toward developing a viscous approach. The discussions that follow this section address the overall computational approach (including grid generation procedures) for predicting subsonic and transonic flow behavior (including shocks) in several high-solidity and high-turning-angle cascade passages. The test cases that were selected for simulation are those blades that were tested under the NASA EEE (Energy Efficient Engine) program[4] and are considered to be representative of advanced turbine technology. In particular, this paper highlights the numerical issues and relevant results of simulating the cascade passages using both an algebraically constructed nonorthogonal H-grid topology and a numerically generated C-grid topology (with a near-orthogonal grid at the cascade surface). The relative merits of the two approaches are discussed here to evolve some basic understanding of the problem. Also reported here are numerical studies that relate to the choice of the artificial damping procedures commonly employed to prevent the appearance of wiggles in regions containing severe pressure gradients in the neighborhood of shock waves or stagnation points and also to prevent wiggles in smooth regions of the flow with large turning angles (e.g., high-turning-angle cascade geometries). The magnitude of the loss in stagnation pressure is utilized to evaluate various available smoothing procedures for such computations.

This paper is divided into several sections. Section II deals with the details of the numerical formulation for the Euler code and the details of the grid generation procedures for the selected test cases. Section III enumerates the various test problems that were analyzed and details the comparisons of the predicted solutions with the measured data for all of the selected test problems. Finally, Sec. IV enumerates some of the important conclusions relevant to the inviscid flow simulation for cascade applications.

II. Numerical Approach

MacCormack's explicit, unsplit time-marching method was utilized to simulate inviscid flow in the cascade geometries of interest. For further details of the scheme, the reader is referred to Refs. 1-3. Highlights of the scheme are outlined below.

Artificial Damping Procedure

To prevent the appearance of wiggles in regions containing severe pressure gradients in the neighborhood of shock waves or stagnation points and also to prevent wiggles in smooth regions of the flow with large turning angles (e.g., high-turning-angle cascade geometries), it has proved necessary to augment the numerical scheme with the addition of an artificial dissipative term. In the past, extensive numerical experiments have been performed to determine a suitable form[3,5,6] for the dissipation term. During our numerical investigation, we experimented with three versions of the dissipation term. The first was that used in our prior attempt,[3] the second form that used by Chima,[5] and the third that used by Jameson et al.[6] Jameson's smoothing approach was found to yield the best performance relative to the numerical error in the stagnation pressure conservation for all of the cascade computations performed.

Boundary Treatments

At the cascade inlet total pressure, total temperature, and the tangential component of velocity (at the inlet boundary) are specified. The normal component of velocity at the inlet

Received July 22, 1985; revision received July 31, 1986.

*Principal Research Scientist. Member AIAA.

†Manager, Turbine Design.

boundary is computed as part of the solution procedure using a local characteristic treatment[3,7] for subsonic inflow conditions.

The downstream boundary is updated by utilizing a combination of extrapolation procedure and specified downstream pressure for subsonic exit flow. No variations in these boundary approaches were investigated, since our previous effort in this area[3] has suggested these procedures to be adequate from a computational efficiency standpoint.

On the blade surfaces, flow tangency is enforced by an even reflection of the tangential velocity from the interior point and an odd reflection of the normal component of velocity. Surface pressures are computed using the normal momentum equation at the wall surface (as discussed in Ref. 3). The wall temperature is found from the surface velocities and the surface total temperature, which must equal the inlet total temperature in steady state. Several variations of these boundary conditions were also attempted to assess their impact on the conservation of total pressure. These approaches basically related to various ways of determining the density/temperature at the wall. Extrapolation of the entropy (expressed as p/ρ^{γ}) or the density from the interior to the wall did not yield any improvement/deterioration of the computed results.

The periodic boundaries are treated by either differencing across the periodic line using the MacCormack's scheme (for H-grid topology) or by an averaging procedure (for C-grid topology) The latter is a convenient way to handle the periodic boundary for C-grid topology offering simplicity in coding procedure.

Grid Generation Procedure

An accurate computation of two-dimensional inviscid flow through cascades of high-solidity and large-camber airfoils, as are found in highly loaded turbine stages, requires a grid topology with several desirable properties. While defining a desirable grid topology is essential for accurate flow computations, generating such a topology that meets all of the requirements is a topic of current research. The grid generator code "GRAPE," originally developed by Sorenson[8] and later modified by Chima[9] for cascade flows, was considered adequate for near-term evaluation. In an effort to develop an understanding of the effect of grid topology on the computed solution for cascade problems, a sheared algebraic grid generator code was also developed. This code generates a nonorthogonal H-grid (commonly known as sheared grid) for blade-to-blade computations.

III. Results and Discussion

The objective of the present paper is to assess the performance of MacCormack's algorithm for the high-turning and high-solidity cascade blades considered to be representative of advanced turbine technology. This numerical algorithm was developed and successfully tested[3] for capturing many physical phenomena that are common to turbomachinery flows (such as shocked flow, shock boundary-layer interaction, separated flow, and turbulence effects). Those test cases, however, were confined to simple geometrical configurations such as flat plates and flat plates with a bump of varying thickness ratio. The intent there was to develop a basic viscous two-dimensional code and to assess its capability relative to the accuracy of the flow predictions.

The issue of accurate simulation of flow containing complex geometries is very closely coupled with the quality of grid topology that is utilized for solving the conservation equations. Grid skewness relative to flow direction, its smoothness, and its aspect ratio all play a very dominant role in generation, distribution, and accumulation of numerical error in a computational procedure. Thus, one attempts to minimize such errors before evaluating an algorithm's capability. There is growing evidence in recent research works[10,11] indicating that the grid generation procedures (and possibly appropriate implementation of boundary conditions) might play a more dominant role than the algorithm itself in contributing to numerical accuracy/inaccuracies of flow computations in the context of a complex physical and geometrical environment. The scope of the present technical effort, however, precluded any substantial effort in the area of grid generation procedures. The technical effort in this phase of the program was structured to evaluate the capability of the numerical algorithm by utilizing available grid generation procedures. As discussed before, the GRAPE code[8,9] was modified and adopted for this purpose. It was, however, considered essential to demonstrate the influence of grid topology for this class of cascade problems in an effort to evaluate and thus recommend future directions. For this reason, an Euler code based on a nonorthogonal H-grid topology (also termed as sheared grid topology) was also developed. C-grid topology (utilizing GRAPE code) was selected for evaluation, since it has distinct advantages over an o-grid topology for viscous flow computations. The technical discussions that follow relate to computational results using both the C- and H-grid topology for all test problems.

Stator Cascade Computations

The first two test cases relate to a turbine stator cascade. In this cascade, the flow enters at zero angle of incidence at low-subsonic flow condition $M \sim 0.1$–0.2 and exits at high-subsonic flow condition $M_e \sim 0.7$–0.9. Further details of these

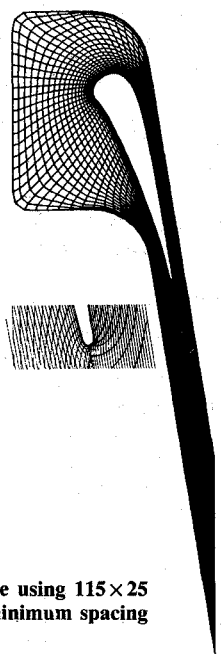

Fig. 1 C-grid topology for stator cascade using 115×25 grid lines, $(J_{te})_{\text{lower}} = 20$, $(J_{te})_{\text{upper}} = 96$, minimum spacing off surface = 0.0035 chord.

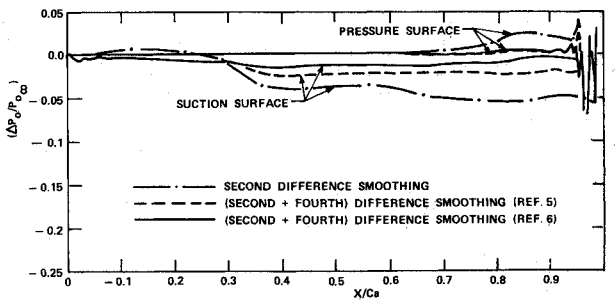

Fig. 2 Influence of smoothing procedures on the predicted numerical error in the conservation of total pressure on the stator airfoil surface at exit Mach number of 0.84 for stator cascade.

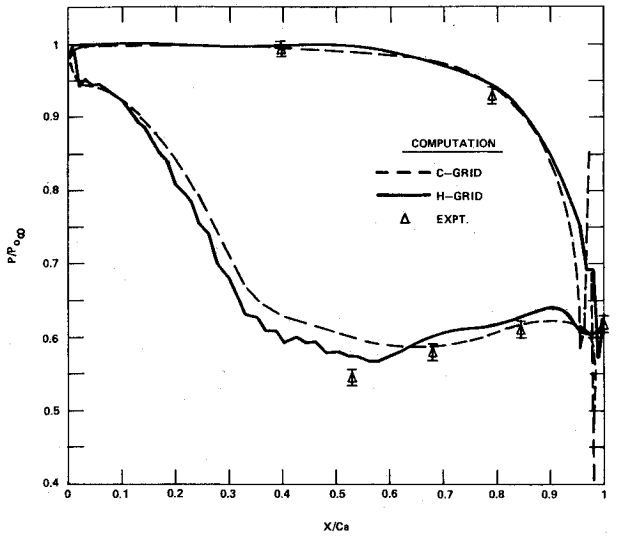

Fig. 3 Predicted surface pressure distribution for stator cascade at exit Mach number of 0.84.

test cases are given in Ref. 4. For this problem, a C-grid topology with 115×25 nodes (Fig. 1) was generated using GRAPE with an initial spacing away from the body of 0.0035 axial chord. In general, an Euler solver is deficient in proper handling of a blunt trailing edge, since there is no physical way to impose the appropriate Kutta condition that can recover the lift associated with such a blade. For all problems studied here, the effect of an unphysical blunt trailing edge was found to be confined near and downstream of this point. The downstream effect was caused by the convection of the spurious entropy generated at the trailing edge.

Stator Cascade Results for Exit Mach Number of 0.84 Using C-grid

The first test case with an inlet Mach number of nearly 0.1 and an area-averaged exit Mach number of 0.84 was selected for extensive numerical experimentation relative to boundary approaches and numerical damping procedures. The intent here was to assess the code performance relative to conservation of mass and stagnation pressure. For this purpose, the number of grid nodes were kept fixed at 115×25 (same as Fig. 1), while a series of runs were made to establish the performance behavior for the Euler code. For all of the cases studied here, the upstream boundary treatment utilized a local one-dimensional characteristics update procedure, the downstream pressure was imposed, and the periodic boundaries were obtained by an averaging procedure. The results of these numerical experimentations are summarized in the following paragraphs.

Of all numerical variations attempted during this effort, the most substantial improvement in stagnation pressure accuracy was obtained by the appropriate choice of the numerical smoothing procedure. Three variations of the numerical smoothing procedures were attempted. These were based on pressure sensors using a second-difference smoothing,[3] a combination of second- and fourth-difference smoothing as implemented by Chima,[5] and a combination of second- and fourth-difference smoothing as implemented by Jameson et al.[6] During these experiments, the numerical error in stagnation pressure conservation at the pressure and suction surfaces was monitored for evaluating the various schemes. The results are shown in Fig. 2. The first procedure utilized in our original Euler code yielded a maximum inaccuracy of nearly 5% on the suction surface and a nearly 2.5% inaccuracy on the pressure surface (excluding the region near the blunt trailing edge) as shown in Fig. 2. This situation was further improved when Chima's procedure[5] was adopted and yielded nearly 2.5% maximum error on the suction surface and virtually none

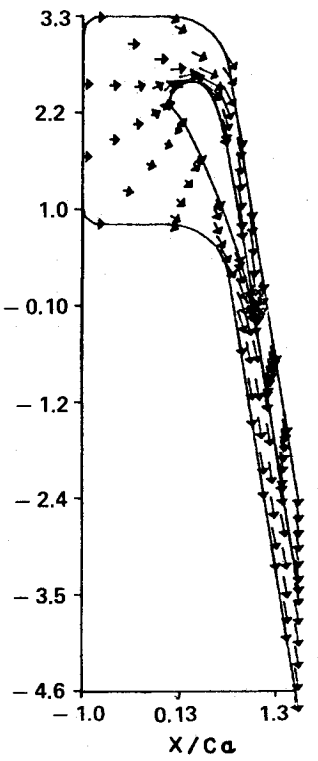

Fig. 4 Velocity vector plot showing computed flowfield for the case shown in Fig. 3 using C-grid.

(~0.2%) at the pressure surface. A further improvement was accomplished when Jameson et al.'s smoothing procedure[6] was adopted in our code. This yielded a maximum error of ~1.5% at the suction surface.

A more careful examination of the results shown in Fig. 2 suggests that for all cases the primary source for numerical entropy generation is on the suction surface at an axial location of $x = 0.3$ measured from the leading edge of the airfoil. Referring to Fig. 1, this location appears to be coincident with high-curvature region on the surface. There can be at least two sources of such numerical errors in a high-curvature region. One of them is an inadequate treatment of the boundary approaches, while the second relates to an inadequate grid resolution in the high-curvature region. A limited attempt was made to reformulate the surface boundary treatments in an effort to identify the source of this problem. These attempts were directed toward such modifications as replacing the specified total surface temperature by an interior extrapolated density or an extrapolated entropy expressed as p/ρ^{γ} and improved evaluation of the curvature term in the normal momentum equation at the surface. No significant improvement in stagnation pressure error was observed due to these efforts.

Figure 3 shows the predicted pressure on the cascade surface as compared to experimental data[4] using Jameson's damping approach. The overall comparison appears to be good except at the suction surface between axial locations at $x = 0.5$–0.6.

Figure 4 shows a vector plot of the entire computational domain for this test case. The essential features of the flow are obvious, such as excessive flow turning on the suction surface near nose region, leading-edge stagnation point location, and fairly uniform exit flow. The details of the computed exit flow for this test case were compared with experiments. These relate to the predicted and measured outflow angle and exit Mach number. The predicted values were computed by averaging in a manner like that used in the experiments, e.g., area-averaged exit Mach number and mass-weighted area-averaged outflow angle. The predicted outflow angle of 10.5 deg compares well with the experimental value 11.0 ± 0.4. The predicted exit flow Mach number of 0.83 compares well with the experimental value 0.84 ± 0.02.

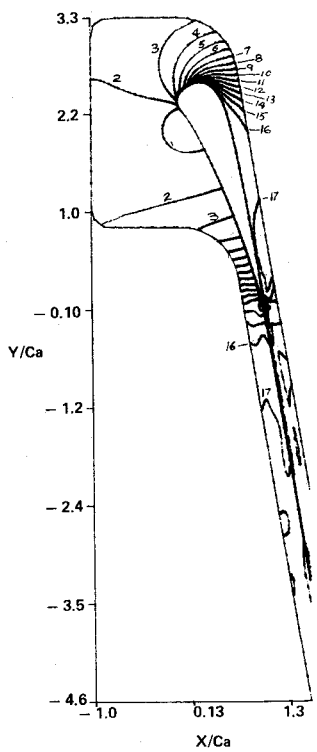

Fig. 5 Predicted Mach number contour lines for the stator cascade at exit Mach number of 0.84 using C-grid topology.

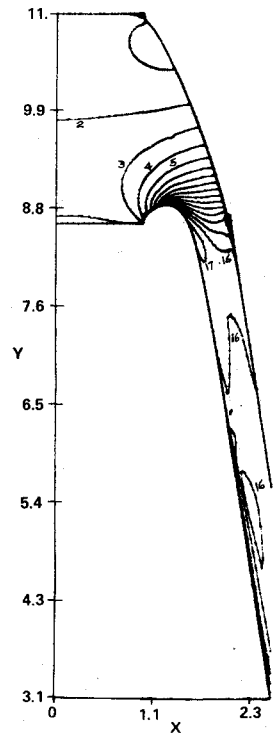

Fig. 6 Predicted Mach number contour lines for the stator cascade at exit Mach number of 0.84 using H-grid topology.

Figure 5 shows the Mach number contour plot for the flow inside the cascade depicting an accelerating flow from a small inlet flow Mach number (~0.1) to the downstream exit Mach number (~0.8) for the entire computational domain. Further detailed comparison with experiments is not possible because such extensive flow information was not obtained during the experimental procedure.

Stator Cascade Results for Exit Mach Number of 0.84 Using H-grid

In an effort to understand the impact of grid topology on the predicted solution for this problem, the Euler code was also exercised using the H-grid system. In this version of the Euler code, all of the numerical formulations are similar to those in the Euler code based on the C-grid. There was also another reason to run this version of the code for all of the test problems, related to the ease of refining the grid size in H-grid topology rather than in C-grid topology. It was found that local grid refinement utilizing the GRAPE code is a particularly tedious (if not difficult) task if the refinement is required at any arbitrary location. In contrast, the sheared grid code is very convenient for doing this. Thus, for this computation, a 100×33 nodes H-topology (with 60 points on each surface as compared to nearly 40 points using C-grid topology) was selected.

The predicted result is shown in Fig. 3. It shows the predicted surface pressure for the cascade as compared to the measured data using the H-grid topology. It is noted here that the grid refinement in the context of this topology has indeed resulted in better comparison with experiments in the region of high curvature (as discussed above).

Figure 6 is a contour plot for the entire computational domain for this computation. Except for minor details at the blunt trailing edge, the overall predicted contour lines compare well with computations based on the C-grid.

Stator Cascade Results for Exit Mach Number of 0.97

In the experimental project[4] the same stator cascade as discussed above was tested at higher exit Mach numbers in an effort to simulate the effect of slight amount of blade twist from the tip to the root section (thus increasing the exit Mach number for the blade). The computational codes were similarly exercised to simulate this effect by appropriately lowering the downstream pressure. For the same grid topology as in Fig. 1, the downstream conditions were changed from $p/p_0 \simeq 0.63$–0.54. The resulting predicted pressure is shown in Fig. 7. Also shown in this figure is the measured data under identical conditions. The predicted pressure once again shows the same trend as in the last case in the high-curvature region of the suction surface. This was anticipated, since no changes in the grid topology were made. The overall computed flow behavior at exit was found to be 10.95 deg as compared to the experimental value of 10.5 ± 0.4 for outflow angle and 0.95 as compared to the experimental value of 0.97 ± 0.02 for exit flow Mach number. The computation also supports the experimental observation that the outflow angle is relatively insensitive to the variation in the exit Mach number for this cascade.

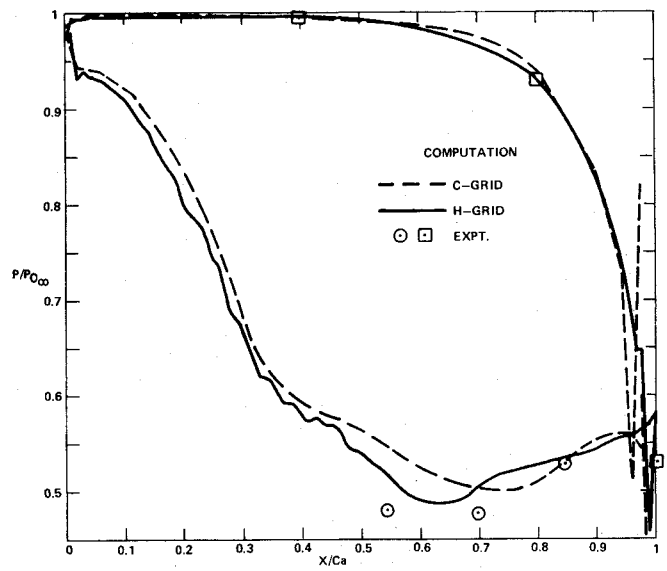

Fig. 7 Predicted surface pressure distribution for stator cascade at exit Mach number of 0.97.

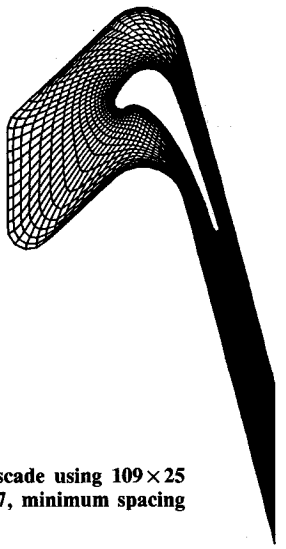

Fig. 8 C-grid topology for rotor cascade using 109×25 grid lines, $(J_{le})_{lower} = 17$, $(J_{te})_{upper} = 97$, minimum spacing off surface = 0.0035 chord.

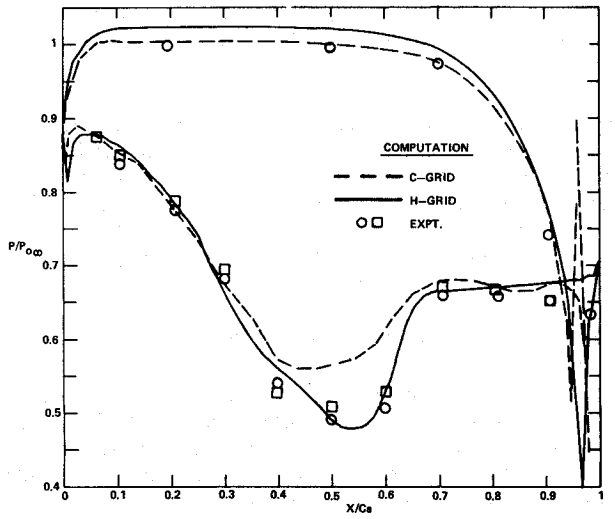

Fig. 9 Predicted surface pressure distribution for rotor cascade at exit Mach number of 0.76.

As before, the same problem was simulated using sheared grid topology. The results so obtained are also presented in Fig. 7 to show the surface pressure. As observed before, the pressure predicted at the suction surface is better than the coarse C-grid topology for the same problem. The other flow properties are as well predicted by the H-grid topology as by the C-grid counterpart.

Rotor Cascade Computations

The next two selected test cases relate to a rotor cascade geometry. These test cases are significantly different from the prior test cases in many ways, such as inlet flow angle, cascade geometry, and test conditions. The discussions that follow will confirm the validity of the Euler codes developed during the technical effort for a wide range of flow conditions and geometrical configurations.

Figure 8 shows the C-grid topology generated by the GRAPE code to simulate the flow details in this cascade. The computational grid consists of 109×25 grid lines in a computational domain consisting of $-1.0 < x < 1.5$ (where x is normalized with the cascade axial chord). A minimum grid spacing of 0.0035 chord length was used as an initial spacing away from the body surface. All attempts were made to obtain a good-quality grid topology within the framework of GRAPE capability. This required several iterative attempts.

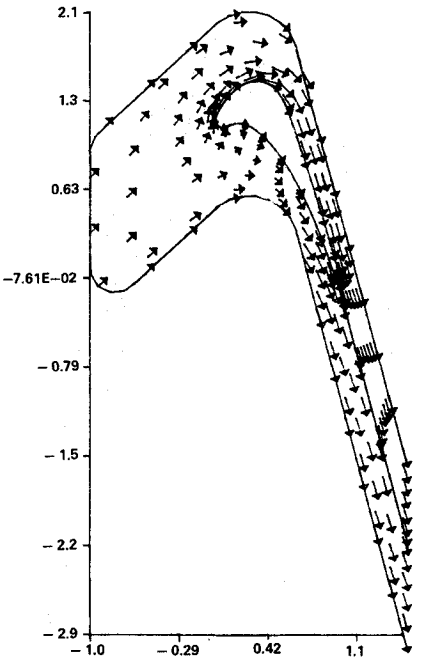

Fig. 10 Predicted velocity vector details for the rotor cascade at exit Mach number of 0.76 using C-grid.

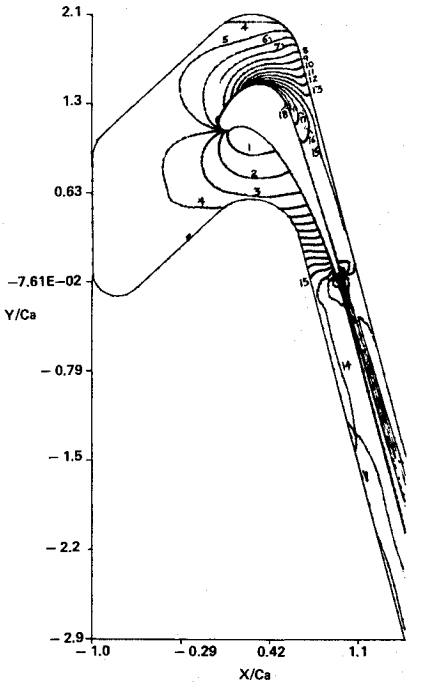

Fig. 11 Predicted Mach number contour lines for the rotor cascade at exit Mach number of 0.76 using C-grid.

Rotor Cascade Results for Exit Mach Number of 0.76 Using C-grid

The Euler code based on C-grid was run for the first test case involving this rotor cascade geometry. This test case corresponds to an inlet incidence angle of 47 deg (measured from the axial direction), an inlet flow Mach number of approximately 0.25, and an exit static to inlet total pressure ratio of ~0.76. An initial guess of uniform flow everywhere based on the inlet conditions was used to start the computational calculations. Figure 9 shows the predicted pressure distribution on the airfoil surface as compared to the experimental data.[4]

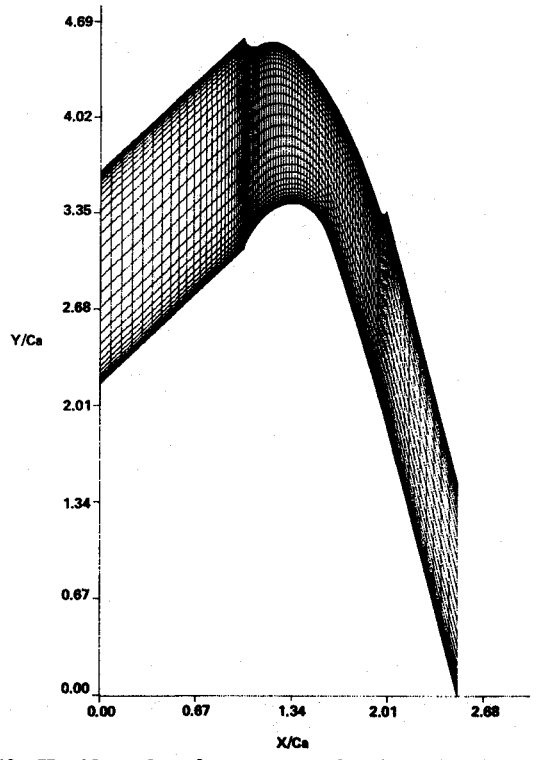

Fig. 12 H-grid topology for rotor cascade using 100×33 grid lines, $J_{le} = 25$, $J_{te} = 85$, minimum $(\Delta x)_{le} = 0.01$, minimum (Δy) at both upper and lower surfaces $= 0.005$.

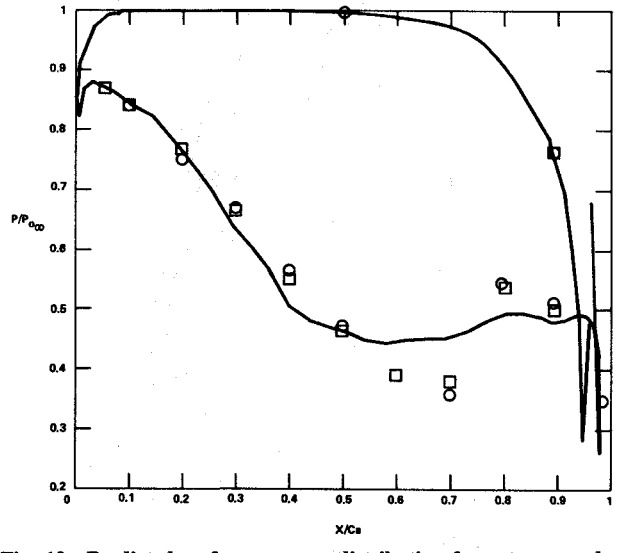

Fig. 13 Predicted surface pressure distribution for rotor cascade at exit Mach number of 1.044 using C-grid topology (solid line is computed result, symbols are experimental data).

The other details of the predicted flow in this cascade at this test condition are shown in Figs. 10 and 11. These are the details of the overall flow behavior in the cascade. For example, Fig. 10 shows the velocity vector plot in the entire computational domain. The location of the stagnation point on the lower surface can be seen by the change in vector direction. Also obvious are the flow acceleration on the upper surface, the large turning angle at the leading edge, and the uniformity of the flow at the exit boundary. Also, for this case, the predicted area-averaged exit Mach number and outflow angle compare very well with the measured data. The measured mass-weighted area-averaged exit flow angle of 14.25 deg was corrected by +2.5 deg by the experimenters due to an experimental error. The new measured value of

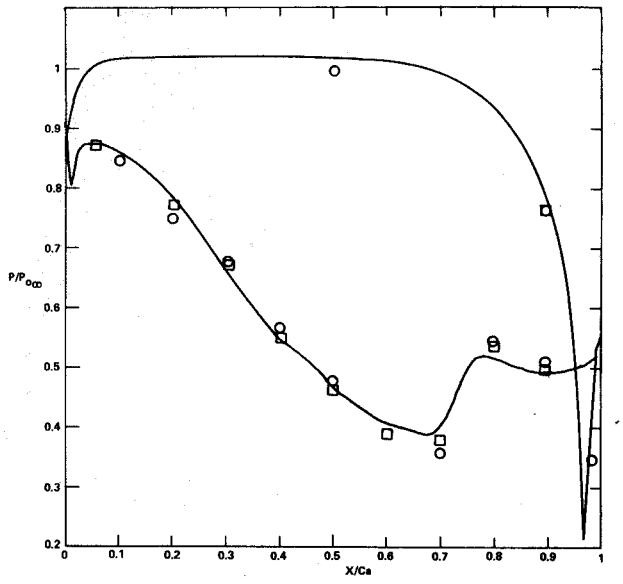

Fig. 14 Predicted surface pressure distribution for rotor cascade at exit Mach number of 1.044 using H-grid topology (solid line is computed result, symbols are experimental data).

16.75 deg compares very closely with the predicted 16.84 deg for this case. Finally, Fig. 11 shows the Mach number contour lines in the entire computational domain. The characteristics of this flow are obvious from this figure, i.e., a major portion of the suction surface near leading edge and a major portion of pressure surface near trailing edge have large amounts of flow accelerations.

Rotor Cascade Results for Exit Mach Number of 0.76 Using H-grid

As outlined before, it was found useful to simulate the foregoing test problem using H-grid topology having a grid that has more resolution than the C-grid system studied before. Figure 12 shows such an H-grid topology for blade-to-blade computation using 100×33 grid lines. This grid topology has 25 expanding x-grid lines upstream (with minimum $\Delta x = 0.01$), 60 x-grid lines on the surface (minimum $\Delta x = 0.01$ at both leading and trailing edges), and the rest in the downstream domain. In the y direction, a minimum grid spacing of $\Delta y = 0.005$ was used on both the upper and lower surfaces. The computational domain was of the same size as in C-grid simulation, i.e., $0 \le x \le 2.5$.

The predicted pressure as shown in Fig. 9 compares well with the experimental data thus indicating the appropriateness of grid resolution for this simulation. The two sets of data shown in Fig. 9 (marked by squares and circles) relate to adjacent cascade passages that indicate the extent of periodicity between the two adjacent flow passages.

Rotor Cascade Results for Exit Mach Number of 1.044

The next test case that was considered for the rotor cascade corresponded to a higher exit Mach number of 1.044 than that of the last case (of 0.76). At this supersonic exit condition, there can be a trailing-edge shock that will reflect off the suction surface of the adjacent blade. According to the flow visualization experiments,[4] the detailed nature of the shock pattern system is dependent on the magnitude of the exit Mach number. At higher supersonic exit Mach numbers, the strength of the trailing-edge shock can be significant. Unfortunately, these experiments did not attempt to gather some quantitative information (in terms of either careful pressure and/or velocity measurements) to address this issue. Schlieren observations reported at exit Mach numbers higher than 1.099 show trailing-edge shock of increasing strength, its interaction with suction surface bound-

ary layer, and subsequent reflected shock-wave pattern. Flow visualizations were also reported indicating possible laminar separation at subsonic exit conditions in the adverse pressure gradient region of the suction surface. These flow visualizations also indicated a second separated zone farther downstream at supersonic exit conditions caused, possibly, by the interaction of the trailing-edge shock from one blade and the boundary layer on the suction surface of the adjacent blade. It is quite obvious that any substantial separation involving either will require a viscous simulation. The good comparisons of the predicted pressure and experimental data at the subsonic exit condition (as reported in the last test case) suggests that the flow separation of the first kind is possibly not very dominant, at least as far as pressure predictions are concerned.

Figure 13 shows predicted pressure on the airfoil surface as compared to the data. It is observed from this figure that, while all of the essential features of the measured surface pressure are present in the predicted pressure, the magnitudes of such pressures are highly diffused. As will become clear later, the difficulty associated with the poor agreement of this simulation with experiments in a high-gradient region of the suction surface has been traced to poor grid resolution in this region. It will be shown later (as in other cases) that a reasonably good comparative agreement with the data can be obtained with appropriate grid refinement using H-grid topology.

The computation predicts mass-weighted, area-averaged exit angle of 17.3 deg as compared to measured value of 17.8 deg and an area-averaged predicted exit Mach number of 0.99 as compared to measured data of 1.04.

This test case was further simulated by using the H-grid topology to assess improvements in the predicted pressure using appropriate grid resolution on the suction surface. The resulting predicted pressure is shown in Fig. 14. It is noted that this predicted pressure is significantly better on the suction surface where rapid variation in pressure occurs, as compared to the coarse C-grid simulation discussed above. The agreement of the predicted pressure with experiments for this case is good.

IV. Conclusions

The important conclusions obtained by computationally simulating several test cases (see Ref. 12 for more details) encompassing subsonic and transonic flow in high-turning-angle and high-solidity cascades can be summarized as follows:

1) Of all smoothing procedures attempted, the Jameson et al. procedure[6] yielded significantly improved stagnation pressure accuracy for all computations. The basic improvement seems to be associated with the addition of a damping term based on the fourth differences in the flux conservations with optimized coefficients. A similar observation is also reported by Rizzi.[13]

2) Of the two grid topologies studied here (C- and H-grid) the C-grid computational approach was found to yield enhanced convergence for identical flow problems. An analysis of the results obtained suggests that such improvements in convergence are bascally realized by proper treatment of the leading and trailing edges in the C-grid topology. Convergence problems with the H-grid topology seem to be associated with skewed grid structure in these regions.

3) A properly resolved (with appropriate grid sizes to resolve high-flow gradients) computational approach based on either C- or H-grid topology can predict overall flow properties reasonably well.

4) The predicted numerical results showed consistently better stagnation pressure accuracy when C-grid topology was used (using the same damping formulation) as compared to the H-grid topology.

5) Of all the airfoil surface boundary conditions attempted, specification of the total wall temperature (in an inviscid model), reflection for tangential and normal velocities in conjuction with normal momentum equation yielded the best numerical results relative to the conservation of total pressure. Further variations of these did not improve the quality of the numerical results.

6) The C-grid computations reported here show a maximum of less than 2% in stagnation pressure error on the airfoil surface and a maximum of less than 1.5% in mass flow error for all stator cascade test cases (excluding regions affected by the blunt trailing edge). For rotor cascade test cases, these numbers are 3% for stagnation pressure error and less than 0.5% in mass flow error.

7) The H-grid computations reported here show a maximum of 3% in stagnation pressure error at the surface and a maximum of 2% in mass flux error (excluding the region affected by the trailing edge) for stator cascade test cases. For rotor cascade test cases, these numbers are 5% for the stagnation pressure error and 1.6% in mass flux error (excluding small leading- and trailing-edge regions).

Acknowledgments

This research was conducted at Avco Everett Research Laboratory Inc. under a subcontract from the Avco Lycoming IRAD Program. The authors wish to thank Avco Lycoming management for financial support and permission to present these results.

References

[1]Srivastava, B.N., "Numerical Solution of the Euler Equations for Turbomachinery Applications, Part I: Inviscid Test Problems," Final Report, Avco Everett Research Laboratory, Everett, MA, Feb. 1984.

[2]Srivastava, B.N., "Numerical Solution of the Thin-Layer Equations for Turbomachinery Applications, Part II: Viscous Test Problems," Final Report, Avco Everett Research Laboratory, Everett, MA, Feb. 1984.

[3]Srivastava, B.N. and Bozzola, R., "Efficient and Accurate Numerical Solutions of the Euler and Navier-Stokes Equations for Turbomachinery Applications," AIAA Paper 84-1300, June 1984.

[4]Kopper, F.C., Milano, R., Davis, R.L., Dring, R.P., and Stoeffler, R.C., "Energy Efficient Engine Component Development and Integration Program," NASA CR-165567, Nov. 1981.

[5]Chima, R.V., "Analysis of Inviscid and Viscous Flows in Cascades with an Explicit Multiple Grid Algorithm," AIAA Paper 84-1663, June 1984.

[6]Jameson, A., Schmidt, W., and Teokel, E., "Numerical Solutions of the Euler Equations by Finite Volume Methods using Runge-Kutta Time-Stepping Schemes," AIAA Paper 81-1259, June 1981.

[7]Jameson, A. and Baker, T.J., "Solution of the Euler Equations for Complex Configurations," AIAA Paper 83-1929, July 1983.

[8]Sorenson, R.L., "A Computer Program to Generate Two-Dimensional Grids about Airfoils and Other Shapes by the use of Poisson's Equation," NASA TM-81198, 1980.

[9]Chima, R., "Modifications to GRAPE Code for Cascades," Private communication, NASA Lewis Research Center, 1984.

[10]Thompkins, W.T. Jr. et al., "Solution Procedures for Accurate Numerical Simulations of Flow in Turbomachinery Cascades," AIAA Paper 83-0257, 1983.

[11]Shyy, W. et al., "A Systematic Comparison of Several Numerical Schemes for Complex Flow Calculations," AIAA Paper 85-0440, 1985.

[12]Srivastava, B.M. and Bozzola, R., "Computation of Flow Fields in High Solidity and High Turning Angle Cascades using Euler Equations," AIAA Paper 85-1705, July 1985.

[13]Rizzi, A., "Spurious Entropy Production and Very Accurate Solutions to the Euler Equations," AIAA Paper 84-1644, June 1984.